



HAL
open science

Alkali-metal electron spin density shift induced by a helium nanodroplet

Markus Koch, Carlo Callegari, Wolfgang E. Ernst

► **To cite this version:**

Markus Koch, Carlo Callegari, Wolfgang E. Ernst. Alkali-metal electron spin density shift induced by a helium nanodroplet. *Molecular Physics*, 2010, 108 (07-09), pp.1005-1011. 10.1080/00268971003623401 . hal-00596286

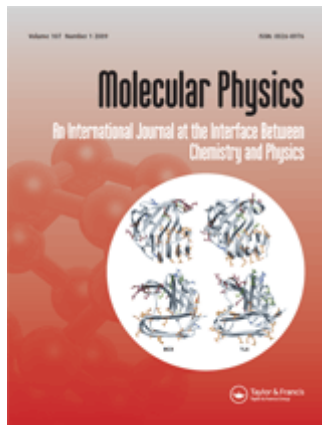
HAL Id: hal-00596286

<https://hal.science/hal-00596286>

Submitted on 27 May 2011

HAL is a multi-disciplinary open access archive for the deposit and dissemination of scientific research documents, whether they are published or not. The documents may come from teaching and research institutions in France or abroad, or from public or private research centers.

L'archive ouverte pluridisciplinaire **HAL**, est destinée au dépôt et à la diffusion de documents scientifiques de niveau recherche, publiés ou non, émanant des établissements d'enseignement et de recherche français ou étrangers, des laboratoires publics ou privés.



Alkali-metal electron spin density shift induced by a helium nanodroplet

Journal:	<i>Molecular Physics</i>
Manuscript ID:	TMPH-2009-0382.R1
Manuscript Type:	Special Issue Paper - In honour of Prof Richard Zare
Date Submitted by the Author:	27-Dec-2009
Complete List of Authors:	Koch, Markus; TU Graz, Institute for Experimental Physics Callegari, Carlo; TU Graz, Institute for Experimental Physics; Sincrotrone Trieste Ernst, Wolfgang; TU Graz, Institute for Experimental Physics
Keywords:	electron spin resonance, optically detected magnetic resonance, helium droplets, magnetic hyperfine structure, alkali-metal atoms
<p>Note: The following files were submitted by the author for peer review, but cannot be converted to PDF. You must view these files (e.g. movies) online.</p> <p>SpinDensityShift.tex Refs.bib</p>	



research article

Alkali-metal electron spin density shift induced by a helium nanodroplet

Markus Koch*, Carlo Callegari**, and Wolfgang E. Ernst

Institute of Experimental Physics, Graz University of Technology, Graz, Austria

(Received 00 Month 200x; final version received 00 Month 200x)

Helium (He) nanodroplets provide a cold and virtually unperturbing environment for the study of weakly bound molecules and van der Waals aggregates. High resolution microwave spectroscopy and the detection of electron spin transitions in doped He droplets have recently become possible. Measurements of hyperfine-resolved electron spin resonance in potassium (^{39}K) and rubidium (^{85}Rb) atoms on the surface of He droplets show small line shifts relative to the bare atoms. These shifts were recorded for all $2I + 1$ components (I is the nuclear spin) of a transition at high accuracy for He droplets ranging in size from 1000 to 15000 He atoms. Evaluation of the spectra yields the influence of the He environment on the electron spin density at the alkali-metal nucleus. A semiempirical model is presented that shows good qualitative agreement with the measured droplet size dependent increase of Fermi contact interaction at the nuclei of dopant K and Rb.

Keywords: electron spin resonance, optically detected magnetic resonance, helium droplets, magnetic hyperfine structure, alkali-metal atoms

1. Introduction

Spectroscopy of doped helium (He) droplets [1] is a well established field of research [2], possibly combining the best aspects of high-resolution spectroscopy and matrix isolation. The latter accounts for the great flexibility of He droplets to cool down almost any conceivable species to 0.38 K, with the ability to synthesize highly unstable atomic and molecular adducts [3, 4]. High resolution—directly reflecting the minimal spectroscopic perturbation due to the He environment—means that those perturbations carry a wealth of information, which remains relatively easy to interpret. Indeed, some of the most exciting findings, such as those related to atomic-scale superfluidity [5–7], physical chemistry studies [8], and synthetic applications [9, 10] are intimately connected to the interpretation of some minute spectral shifts. Due to their ability to act as a thermostat at very low temperature, He nanodroplets naturally facilitate the alignment of an electric [11] or magnetic [12] dipole carried by the dopant, by means of an external field.

In the gas phase, the use of polarized light to detect the alignment and orientation of molecules has been pioneered and thoroughly investigated by Zare and coworkers [13, 14], as have been level crossing spectroscopy [15, 16], and optical pumping [17, 18]. High resolution spectroscopy and detailed hyperfine studies [19]

*Corresponding author. Email: markus.koch@tugraz.at

**Present address: Sincrotrone Trieste, Strada Statale 14 - km 163.5, 34149 Basovizza, Trieste, Italy

provided the basis for the state selective detection in crossed molecular beam studies [20] and the interpretation of the corresponding reaction dynamics [21, 22]. Many of the classic schemes of high resolution spectroscopy have been successfully applied to doped He nanodroplets, including double-resonance [23–26], and the use of selection rules for polarized light in combination with external electric [4] and magnetic [27] fields.

We have previously performed a whole series of experiments on the valence-electron spin of potassium (K) and rubidium (Rb) atoms [27, 28], dimers [27], and trimers [29] on He droplets in a strong magnetic field. These have culminated in the successful implementation of optically detected magnetic resonance (ODMR), and we have been able to recently report the first observation of hyperfine-resolved electron spin resonance (ESR) spectra of K and Rb on the surface of He nanodroplets [30, 31], with such high resolution that shifts could be followed as a function of droplet size for ^{85}Rb atoms, despite the fact that they amount to few parts per million only. Previously electron- and nuclear-spin spectroscopy of alkali-metal atoms were performed in bulk superfluid and solid He matrices [32–34] at lower experimental accuracy, so that the effect of the He, although larger, was hardly quantifiable.

In this manuscript we present a detailed set of hyperfine-resolved ESR spectra of ^{85}Rb atoms on He nanodroplets, investigated as a function of the mean droplet size \bar{N} . The positions of the $2I + 1$ lines of the multiplet (I being the nuclear spin quantum number of the atom) can be reproduced with the standard Breit–Rabi formula [35], provided that its two main parameters (g_J , a_{HFS} , see below) are allowed to slightly differ from the well known values [36] of the bare atom. *A posteriori* it is the change of a_{HFS} which is responsible for the observed spectral shifts; this can be rationalized by invoking a slight compression of the valence-electron wavefunction of the atom, hence an increase of the Fermi contact interaction. We support this conclusion with a simple model where the effect is semiempirically estimated based on computed He densities and electron wavefunctions; the model correctly predicts the magnitude of the minute change of a_{HFS} , as well as the trend versus \bar{N} . The manuscript is organized as follows: Section 2 presents the experimental apparatus and Section 3 the experimental spectra and their fit to the Breit–Rabi formula. The extracted hyperfine parameters as a function of \bar{N} and the semiempirical model for δa_{HFS} are explained in Section 4. Section 5 presents the conclusions and a summary.

2. Experiment

A complete description of the experimental setup is given elsewhere [31]. In brief, He droplets are produced via supersonic expansion of grade-6 He gas through a cold nozzle into vacuum (nozzle diameter $5\ \mu\text{m}$, $T = 12.5\text{--}23\ \text{K}$, stagnation pressure 50 bar, mean droplet size $\bar{N} \approx 1000\text{--}15000$ He atoms). Figure 1 shows a schematic diagram of the setup. The droplet beam is doped with, on average, one Rb atom per droplet in a heatable pickup cell, which is loaded with Rb metal. Inside the homogeneous magnetic field region (B_0) of an electromagnet the droplet beam is crossed by the pump and the probe laser beams. A microwave (MW) cavity, with entrance and exit holes for the droplet beam, is located between the two laser beams. The pump laser beam creates a net polarization in the orientation of the Rb valence-electron spin which is then coherently manipulated with the resonant microwave field. Laser-induced fluorescence (LIF) is collected at the intersection of the droplet beam with the probe laser beam, and detected by a photomultiplier tube. Electron spin resonance (ESR) transitions are detected indirectly as an in-

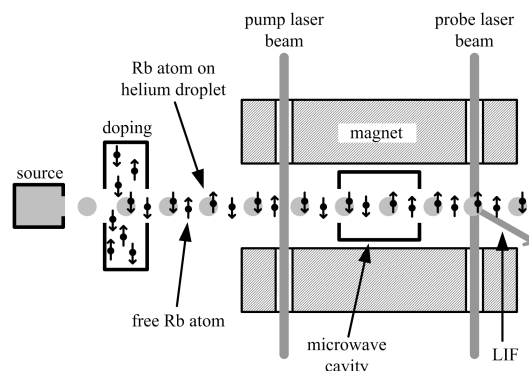


Figure 1. Schematic diagram of optically detected magnetic resonance (ODMR) of Rb atoms on He droplets. The circularly polarized pump laser beam, tuned to the $5^2P_{1/2} \leftarrow 5^2S_{1/2}$ transition, only excites spin-up atoms, which relax back to $5^2S_{1/2}$ without desorbing and in a random spin state. Thus optical pumping is established and a net spin-down polarization is established in an initially unpolarized ensemble. Electron spin resonance (ESR), induced with resonant microwave radiation, is detected indirectly with the circularly polarized probe laser beam, based on the fact that laser-induced fluorescence (LIF) is only obtained from spin-up atoms.

crease of LIF signal when B_0 is scanned into resonance at fixed MW frequency ν_0 . A direct detection of spin transitions is impossible due to the low optical density of the droplet beam. This ODMR scheme is the key that makes ESR spectra of doped He droplets possible.

Selective addressing of different hyperfine states [37] by single-frequency lasers, as ODMR is usually achieved, is not possible on He droplets because of a significant line broadening of electronic transitions due to perturbation of the droplet [38, 39]. However, Zeeman sublevels can still be individually addressed by means of selection rules for circularly polarized light. The differential absorption of left- and right-circularly polarized light (magnetic circular dichroism, MCD) is used to create a net spin polarization as well as to quantify it.

The pump and the probe laser beams are obtained from the same cw Ti:Al₂O₃ ring laser; they are both circularly polarized, with same helicity. The laser is tuned to the wavelength with the most efficient spin polarization and spin probe action (12601 cm⁻¹ for Rb, 12993 cm⁻¹ for K) [31]. For Rb this is roughly the maximum of the droplet broadened line of the D₁ transition ($5^2P_{1/2} \leftarrow 5^2S_{1/2}$), whereas for K the optimum spin polarization/probe action is at lower excitation energy than the center of the droplet broadened D₁ line ($4^2P_{1/2} \leftarrow 4^2S_{1/2}$) [31].

Rb atoms stay on the droplet upon excitation [28], so the pump laser creates a net spin polarization through spin pumping. K atoms, in contrast, detach from the droplet upon excitation [27] so the net spin polarization is obtained through depleting the undesired spin state.

The magnetic field is measured with a commercial nuclear magnetic resonance magnetometer a few centimeters away from the MW cavity. An unwanted gradient of B_0 makes this value differ from the field value inside the cavity; this means that we do not know B_0 exactly in the region where the spin manipulation takes place. We use, therefore, a second laser to create an ODMR reference signal from gas phase Rb atoms, which are effusing from the pickup cell in addition to the doped droplets (see Figure 1). A grating-stabilized, single-mode diode laser is tuned to the Rb gas-phase D₁ transition (12578.950 cm⁻¹ [40]), split and polarized in the same fashion as the Ti:Al₂O₃ laser beams, and collinear to them. Since the two lasers are used simultaneously, a magnetic field scan results in two ESR peaks, one due to the gas-phase Rb atoms (the free-atom peak) and one due to the Rb atoms attached to a droplet (the on-droplet peak, see Section 3, Figure 3). The data points, depicting the observed change of LIF signal, are fitted with a Gaussian function: the shift

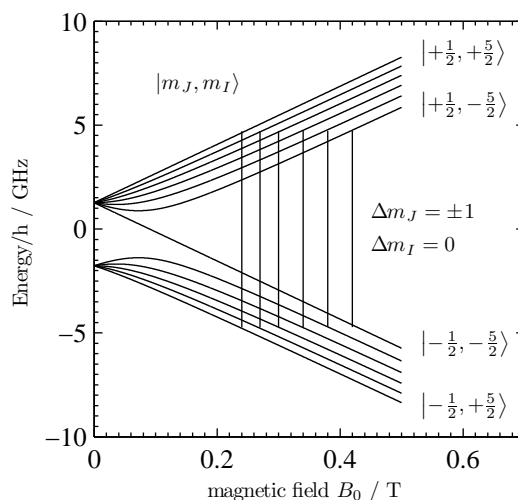


Figure 2. Energy diagram of the hyperfine levels of ^{85}Rb (nuclear spin $I = 5/2$) in its electronic ground state ($^2S_{1/2}$) versus the magnetic field B_0 , as calculated with the Breit–Rabi formula [35]. The vertical lines indicate the six possible ESR transitions ($\Delta m_J = \pm 1$, $\Delta m_I = 0$) for a fixed microwave frequency of $\nu_0 = 9.44229$ GHz.

of the on-droplet peak with respect to the free-atom peak is immediately apparent for all ESR transitions. These line shifts are induced by the He environment of the droplet and are accurately reproducible.

The actual free-atom ESR positions (the values of B_0 at which the free-atom ESR transitions occur for a given ν_0) are calculated with the Breit–Rabi formula [35] using the known values of the hyperfine constant a_{HFS} , the Landé factor g_J , and the nuclear factor g_I [36].

Adding the observed line shifts to these free-atom ESR positions gives the exact on-droplet ESR line positions. All on-droplet line positions are then fitted at once using the Breit–Rabi formula again, this time allowing a_{HFS} and g_J to differ by δa_{HFS} ($= a_{\text{HFS, droplet}} - a_{\text{HFS, free}}$) and δg_J ($= g_{J, \text{droplet}} - g_{J, \text{free}}$) respectively; g_I is kept unchanged.

For K, in contrast, the shifts are not large enough that a free-atom peak and the related on-droplet peak can be resolved. In this case, the two lasers are alternately blocked, and the two ESR peaks are measured in sequence. This relies on the reproducibility of a B_0 scan as a function of the voltage supplied to the scanning coils. We tested very thoroughly the reproducibility to hold for the small scanning ranges involved.

3. Results

In this work, the droplet size dependence of the hyperfine resolved ESR spectrum of ^{85}Rb atoms on He droplets has been investigated in detail. ^{85}Rb has a nuclear spin of $I = 5/2$, and the six possible magnetic quantum numbers (the projection of the nuclear spin along the quantization axis given by B_0) are $m_I = \pm 5/2$, $\pm 3/2$, and $\pm 1/2$, as indicated in Figure 2. The six possible ESR transitions are given by the selection rules $\Delta m_I = 0$ and $\Delta m_J = \pm 1$. A full ESR spectrum of ^{85}Rb atoms on He_N ($N \approx 8000$) was presented recently [30]. The hyperfine constant was found to be increased by $\delta a_{\text{HFS}} \approx 400$ ppm, while the Landé factor g_J remained unchanged within the experimental uncertainties, a few ppm.

Figure 3 shows the lowest field on-droplet ESR transition ($m_I = +5/2$) for

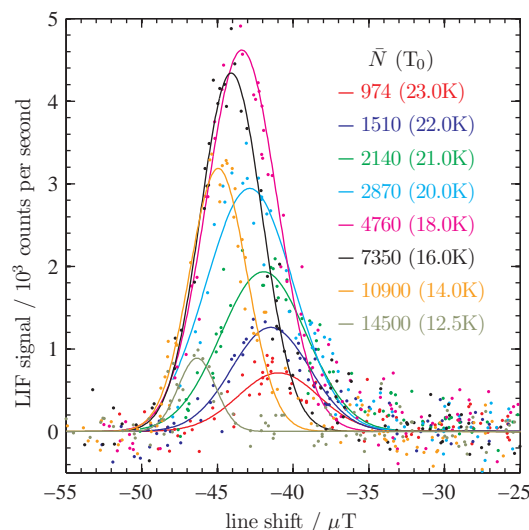


Figure 3. Shift of the lowest-field on-droplet ESR transition of ^{85}Rb atoms ($I = 5/2$, $\Delta m_J = \pm 1$, $m_I = +5/2$) on He droplets with different droplet sizes. The data points are fitted with Gaussian functions. The droplet sizes and the corresponding nozzle temperatures (in brackets) are given in the legend. The free-atom peak occurs at $B_0 = 0.241544\text{ T}$ ($\nu_0 = 9.44229\text{ GHz}$) and the individual line shifts are (from smaller to larger droplets): $\Delta B = -41.0(5)$, $-41.5(3)$, $-41.9(3)$, $-42.9(3)$, $-43.4(3)$, $-44.1(2)$, $-44.9(2)$, $-46.3(3)\ \mu\text{T}$ (experimental error given in parentheses).

Table 1. Free-atom absolute line position B_0 , and on-droplet line shift ΔB_{22} for a nozzle temperature of $T_0 = 22\text{ K}$, and ΔB_{13} for $T_0 = 13\text{ K}$ according to Figure ?? (for $T_0 = 13\text{ K}$ and 22 K). The microwave frequency was $\nu_0 = 9.44212\text{ GHz}$. The experimental error in the last digit of the line shift is given in parentheses.

m_I	+5/2	+3/2	+1/2	-1/2	-3/2	-5/2
B_0/T	0.241538	0.269756	0.301897	0.338108	0.378391	0.422594
$\Delta B_{22}/\mu\text{T}$	-40.8(9)	-33.3(7)	-22.8(7)	-8.1(6)	+8.5(5)	+29.4(4)
$\Delta B_{13}/\mu\text{T}$	-44.7(5)	-36.5(7)	-24.7(6)	-9.5(6)	+9.6(8)	+33.1(3)

different droplet sizes. The free-atom peak occurs at $B_0 = 0.241544\text{ T}$ ($\nu_0 = 9.44229\text{ GHz}$) and individual line shifts are given in the figure caption. The different droplet sizes, ranging from ~ 1000 to ~ 15000 He atoms per droplet, are obtained with nozzle temperatures in the range of 23 to 12.5 K. All droplet sizes stated here are assigned using data from the literature [41]. Since no droplet sizes are reported for the nozzle pressure we used (50 bar), the closest available data are taken (40 bar). The values of \bar{N} are mean values; the spread of the distribution ($N_{1/2}$, width at half maximum) is comparable to the mean droplet size: Harms, Toennies, and Dalfovo [41] give, e.g., $N_{1/2} = 4160$ for $\bar{N} = 4700$.

Figure ?? shows the relative line position of all six hyperfine transitions obtained with small (orange) and large (blue) droplets (only the fit curves are shown, for clarity); a free atom peak (red), which appears per definition at zero line shift, is also shown. The relative line position of all six hyperfine transitions obtained with small ($\bar{N} \approx 1510$, $T_0 = 22\text{ K}$) and large ($\bar{N} \approx 13200$, $T_0 = 13\text{ K}$) droplets are listed in Table 1. The influence of smaller droplets ($\bar{N} \approx 1510$, $T_0 = 22\text{ K}$) is clearly less than the influence of bigger droplets. ($\bar{N} \approx 13200$, $T_0 = 13\text{ K}$). The corresponding values for B_0 and ΔB are listed in Table 1. Note that the line positions for ^{87}Rb atoms ($I = 3/2$, $\nu_0 = 9.442\text{ GHz}$) are 0.1136, 0.1816, 0.3076, and 0.4918 T so that there is no interference between the two isotopes in the detected signal.

Full ESR spectra are recorded for the five different nozzle temperatures

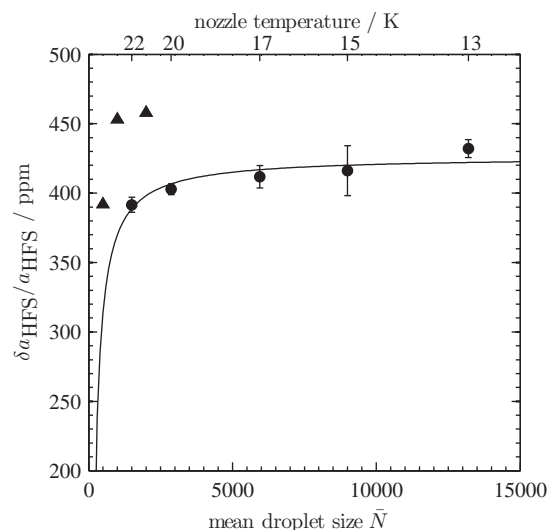


Figure 4. Relative change of the hyperfine constant $\delta a_{\text{HFS}}/a_{\text{HFS}}$ ($\delta a_{\text{HFS}} = a_{\text{HFS, droplet}} - a_{\text{HFS, free}}$) as a function of the droplet size \bar{N} for ^{85}Rb atoms on He droplets. The corresponding nozzle temperatures are reported on the top axis. The solid line represents a $1/N$ dependence of the form $\frac{\Delta a_{\text{HFS}}}{a_{\text{HFS}}} = 426(17) - 6(5) \cdot 10^4 N^{-1}$ (standard error given in parentheses), which serves as a guide to the eye. Computed values (see Table 2) are indicated by triangles.

$T_0 = 13, 15, 17, 20,$ and 22 K, corresponding to mean droplet sizes in the range of 13200 to 1510 He atoms per droplet. For each spectrum the change of the hyperfine constant δa_{HFS} is determined by fitting all six individual on-droplet ESR peaks at once with the Breit–Rabi formula (the Landé factor g_J remains unchanged). The relative change $\delta a_{\text{HFS}}/a_{\text{HFS}}$ as a function of the droplet size \bar{N} is shown in Figure 4. The solid line represents a $1/N$ dependence, which serves as a guide to the eye, and an extrapolation to infinite droplet size gives a limit of $\delta a_{\text{HFS}}/a_{\text{HFS}} = 426(17)$ ppm. The solid line represents a dependence of the hyperfine constant on the droplet size of the form $\frac{\Delta a_{\text{HFS}}}{a_{\text{HFS}}} = 426(17) - 6(5) \cdot 10^4 N^{-1}$ (standard error given in parentheses). The limit for $N \rightarrow \infty$ corresponds to a single Rb atom on a flat liquid helium surface.

4. Interpretation

A new perturbational approach has recently been taken for the calculation of potential energy curves of an alkali-metal atom A on a He nanodroplet as a function of the distance R_A between the atom and the center of the droplet [42]. With their method, Callegari and Ancilotto computed for droplet sizes $N = 500, 1000,$ and 2000 He atoms:

- (1) the potential energy curve $V_0(R_A)$ of the ground electronic state of A as a function of the distance R_A , and the corresponding wavefunction $\phi_0(R_A)$ in the ground vibrational state supported by this potential energy curve; $|\phi_0(R_A)|^2$ describes the probability of finding A at distance R_A from the droplet in the simplifying assumption that the droplet has no internal degrees of freedom.
- (2) the He density $\rho_0(R, \Theta)$ at equilibrium in the external potential of an alkali-metal atom A. The latter is taken to be the He–A pair potential calculated by Patil [43]. R, Θ are radial and polar spherical coordinates centered on the droplet.

(3) the perturbed wavefunction of the electronic ground state of the alkali-metal atom $\Psi'_{n'00}(R_A, r, \theta) = \sum_{n,l} c_{nl0}(R_A)\Psi_{nl0}(r, \theta)$ expressed in a basis of “exact” (for a chosen effective potential) valence-electron wavefunctions $\Psi_{nlm}(r, \theta)$ for the bare atom A; r and θ are radial and polar spherical coordinates centered on A; n, l, m are the standard principal, azimuthal, and magnetic quantum numbers. While n, l no longer are good quantum numbers, the label $\Psi'_{n'00}$ is meant to reflect the fact that $c_{n'00}$ ($n' = 4, 5$ respectively for K, Rb) is by far the leading coefficient for all R of interest; because of cylindrical symmetry, m remains strictly conserved.

Following Adrian [44], the relative change $\delta a_{\text{HFS}}/a_{\text{HFS}}$ is calculated for every given value of R_A as the change of valence-electron density at the nucleus ($r = 0$; note that θ is redundant for $r = 0$)

$$\left. \frac{\delta a_{\text{HFS}}}{a_{\text{HFS}}} \right|_{\text{Pauli}} = \frac{|\Psi'_{n'00}(R_A, 0, \theta)|^2}{|\Psi_{n00}(0, \theta)|^2} - 1 \quad (1)$$

For the values of R_A of interest, Equation 1 is positive and expresses the slight compression of the valence-electron wavefunction, as expected. The subscript $|_{\text{Pauli}}$ reflects the fact that in the derivation of the valence-electron wavefunction, the model of Callegari and Ancilotto [42] properly accounts for repulsive forces (Pauli forces between He and A), but neglects the effect of van der Waals forces on the wave function. To account for the van der Waals contribution to $\delta a_{\text{HFS}}/a_{\text{HFS}}$, we apply an empirical correction in the spirit of the one proposed by Adrian [44]. Our correction is: Compared to Adrian’s Equation (10) we have to replace his parameter E_V by a term integrating over the helium density distribution. Thus we obtain:

$$\left. \frac{\delta a_{\text{HFS}}}{a_{\text{HFS}}} \right|_{\text{vdW}} = - \left(\frac{2}{E_A} + \frac{1}{E_A + E_{\text{He}}} \right) \int_V \frac{f_6(|\vec{R}_A - \vec{R}|) C_6 \rho_0(\vec{R})}{|\vec{R}_A - \vec{R}|^6} d\vec{R} \quad (2)$$

where the integration domain V is the whole space (computationally, the grid over which ρ_0 is defined), f_6 and C_6 are as defined by Patil [43]. E_A, E_{He} are the average excitation energies of the bare alkali-metal atom and the bare He atom, respectively, are expressed in atomic units, and are positive in this context, so that the correction is negative.

Values for E_A and E_{He} are average excitation energies, calculated as the average of the energy of the first excited state and the ionization energy [40]. In this way, we arrive at $E_{\text{He}} = 179083 \text{ cm}^{-1}$, $E_{\text{K}} = 24017 \text{ cm}^{-1}$, and $E_{\text{Rb}} = 23214 \text{ cm}^{-1}$ for He, K, and Rb, respectively.

Note that this acts to compensate the positive change due to Pauli forces which alone is much larger than the experimentally measured value. The total calculated change is:

$$\frac{\delta a_{\text{HFS}}}{a_{\text{HFS}}} = \left. \frac{\delta a_{\text{HFS}}}{a_{\text{HFS}}} \right|_{\text{Pauli}} + \left. \frac{\delta a_{\text{HFS}}}{a_{\text{HFS}}} \right|_{\text{vdW}} \quad (3)$$

Note that over the range of R_A where the probability of finding A is still significant, $\delta a_{\text{HFS}}/a_{\text{HFS}}$ varies much more than the linewidth we experimentally observe; if $|\phi_0(R_A)|^2$ were a static distribution, this would result in a broad ESR line. From this we deduce that we ought to apply motional narrowing [45], which is reasonable considering that the frequency of the vibrational motion along R_A is an order

Table 2. Contributions in parts per million to $\overline{\left(\frac{\delta a_{\text{HFS}}}{a_{\text{HFS}}}\right)}$ for K and Rb atoms on He droplets. N is the number of He atoms per droplet.

N	Pauli	van der Waals	Pauli + van der Waals
K			
500	+1630	-1294	+336
1000	+1831	-1464	+367
2000	+1928	-1558	+370
Rb			
500	+1838	-1446	+392
1000	+2151	-1698	+453
2000	+2270	-1812	+458

of magnitude larger than the microwave frequency. We thus calculate an average value

$$\overline{\left(\frac{\delta a_{\text{HFS}}}{a_{\text{HFS}}}\right)} = \int \frac{\delta a_{\text{HFS}}}{a_{\text{HFS}}} |\phi_0(R_A)|^2 dR_A \quad (4)$$

which corresponds to the values tabulated, in parts per million, in Table 2. The values for Rb are indicated by triangles in Figure 4.

In Ref. [30] we have reported preliminary calculations for Rb where we have inadvertently swapped the roles of E_A and E_{He} in Equation 2 with the result that the prefactor in front of the integral in Equation 2 appears to be an order of magnitude smaller than it actually is, and the van der Waals contribution has almost no influence. Therefore, the values of $\delta a_{\text{HFS}}/a_{\text{HFS}}$ were larger by a factor of 4, almost the size of the value of the Pauli column in Table 2.

5. Conclusions and summary

Applying ODMR spectroscopy to alkali-metal atoms on the surface of He nanodroplets, we were able to record hyperfine-resolved electron spin resonance transitions at a high enough precision to determine the droplet size dependent Fermi contact interaction of the valence electron at the alkali-metal nucleus. In order to account for the physics behind the electron spin density shift induced by the He environment, we developed a model in the spirit of the work by Adrian [44]. Using the results of Callegari and Ancilotto [42] for the potential energy curves of the ground and excited states of alkali-metal atoms as a function of their distance to the droplet center and the corresponding He density, the value of the perturbed valence-electron wavefunction at the nucleus in the alkali-metal ground state was computed. The influences both of the repulsive Pauli forces and the attractive van der Waals interactions were taken into account yielding relative shifts in reasonable agreement with the measurements. The interaction of the alkali-metal atom with the He increases with droplet size and the change of hyperfine shift correspondingly increases. The most obvious manifestation of this is an increasingly deeper dimple in the surface of the He droplet. Let us note that the maximum shift would be expected with the alkali-metal atom located in the center of the droplet; this energetically unstable configuration would give results similar to those of experiments in bulk He, where much larger shifts are indeed observed. At the moment we are not in the position to separately quantify the role of an increased local density in the vicinity of the atom, of a flatter radius of curvature of the droplet, and of a larger depth of the dimple, all three of which can be expected to contribute a larger

1 shift. Of course semiempirical models have to be tested carefully and should be
 2 applied to more data sets than currently available. With corrective terms of simi-
 3 lar size and opposite signs, there is a danger that the final result depends strongly
 4 on the input data for one or the other term. Here, we consistently used the adia-
 5 batic potentials for alkali-metal–inert gas systems in the ground state by Patil [43].
 6 Kleinekathöfer, Lewerenz, and Mladenović [46] apply a slightly different form of
 7 potential for alkali-metal–He pairs and list corresponding parameters. Their values
 8 for f_6 and C_6 differ from those of Patil but should only be used in our Equation 2 if
 9 the droplet–alkali-metal potential and the wavefunctions were also modelled with
 10 these data. Considering these uncertainties, one of the strong points of our model
 11 lies in the fact that it shows the correct relative trend for the spin densities as
 12 function of the droplet size.

13
 14 In the near future, we will extend our measurements of alkali-metal spin densities
 15 to He droplets loaded with different dopants that reside in the center of the droplet,
 16 testing the interaction between the nuclear spin of a “center dopant” with the
 17 valence electron of the “surface dopant”.

18
 19
 20
 21
 22 **6. Acknowledgments**

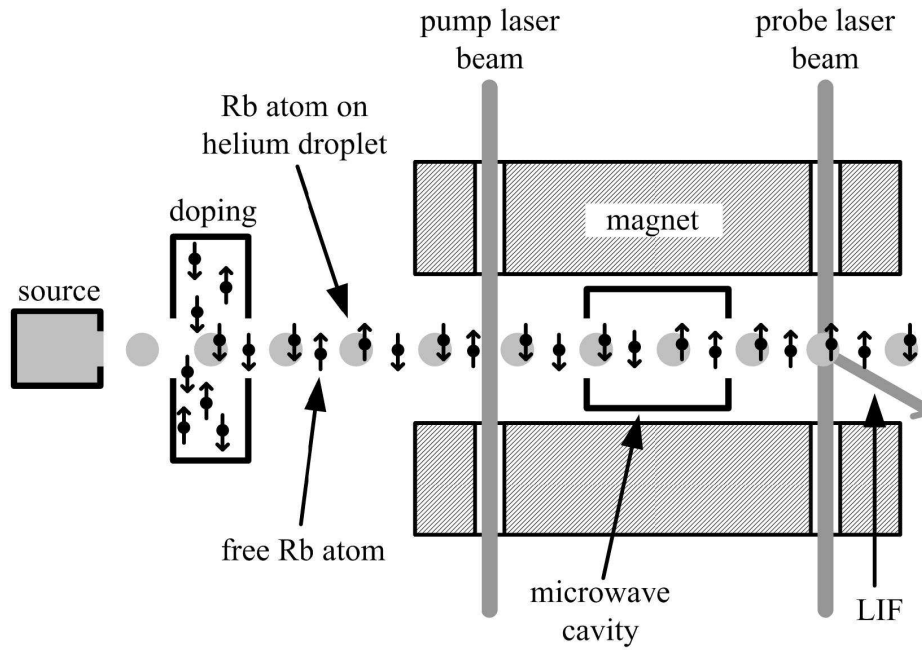
23 We thank F. Ancilotto for calculating the He droplet densities, and A.W. Hauser
 24 and K.K. Lehmann for helpful discussions. This research was supported by the
 25 Austrian Science Fund (FWF) under Grant No. P18053-N02.

26
 27
 28
 29 **References**

30
 31 [1] S. Goyal, D.L. Schutt and G. Scoles, *Phys. Rev. Lett.* **69** (6), 933–936 (1992).
 32 [2] J.P. Toennies and A.F. Vilesov, *Angew. Chem.-Int. Edit. Engl.* **43** (20), 2622–2648 (2004).
 33 [3] J. Higgins, C. Callegari, J. Reho et al., *Science* **273** (5275), 629–631 (1996).
 34 [4] K. Nauta and R.E. Miller, *Phys. Rev. Lett.* **82** (22), 4480–4483 (1999).
 35 [5] M. Hartmann, F. Mielke, J.P. Toennies et al., *Phys. Rev. Lett.* **76** (24), 4560–4563 (1996).
 36 [6] S. Grebenev, J.P. Toennies and A.F. Vilesov, *Science* **279** (5359), 2083–2086 (1998).
 37 [7] J. Tang, Y.J. Xu, A.R.W. McKellar and W. Jäger, *Science* **297** (5589), 2030–2033 (2002).
 38 [8] M.Y. Choi, G.E. Douberly, T.M. Falconer et al., *Int. Rev. Phys. Chem.* **25** (1-2), 15–75 (2006).
 39 [9] J. Küpper and J.M. Merritt, *Int. Rev. Phys. Chem.* **26** (2), 249–287 (2007).
 40 [10] A. Gutberlet, G. Schwaab, O. Birer et al., *Science* **324** (5934), 1545–1548 (2009).
 41 [11] K. Nauta and R.E. Miller, *Science* **283** (5409), 1895–1897 (1999).
 42 [12] G. Auböck, J. Nagl, C. Callegari and W.E. Ernst, *J. Phys. Chem. A* **111** (31), 7404–7410 (2007).
 43 [13] C.H. Greene and R.N. Zare, *J. Chem. Phys.* **78** (11), 6741–6753 (1983).
 44 [14] R. Altkorn and R.N. Zare, *Annu. Rev. Phys. Chem.* **35**, 265–289 (1984).
 45 [15] D.R. Crosley and R.N. Zare, *Phys. Rev. Lett.* **18** (22), 942–944 (1967).
 46 [16] J. Mills and R. Zare, *Chem. Phys. Lett.* **5** (1), 37–41 (1970).
 47 [17] R.E. Drullinger and R.N. Zare, *J. Chem. Phys.* **51** (12), 5532–5542 (1969).
 48 [18] ———, *J. Chem. Phys.* **59** (8), 4225–4234 (1973).
 49 [19] W.E. Ernst, J. Kändler, C. Noda et al., *J. Chem. Phys.* **85** (7), 3735–3743 (1986).
 50 [20] P.H. Vaccaro, D. Zhao, A.A. Tsekouras et al., *J. Chem. Phys.* **93** (12), 8544–8556 (1990).
 51 [21] P.H. Vaccaro, A.A. Tsekouras, D. Zhao et al., *J. Chem. Phys.* **96** (4), 2786–2798 (1992).
 52 [22] K.S. Kalogerakis and R.N. Zare, *J. Chem. Phys.* **104** (20), 7947–7964 (1996).
 53 [23] I. Reinhard, C. Callegari, A. Conjusteau et al., *Phys. Rev. Lett.* **82** (25), 5036–5039 (1999).
 54 [24] C. Callegari, I. Reinhard, K.K. Lehmann et al., *J. Chem. Phys.* **113** (11), 4636–4646 (2000).
 55 [25] S. Grebenev, M. Havenith, F. Madeja et al., *J. Chem. Phys.* **113** (20), 9060–9066 (2000).
 56 [26] G.E. Douberly, J.M. Merritt and R.E. Miller, *Phys. Chem. Chem. Phys.* **7**, 463–468 (2005).
 57 [27] J. Nagl, G. Auböck, C. Callegari and W.E. Ernst, *Phys. Rev. Lett.* **98** (7), 075301–1–4 (2007).
 58 [28] G. Auböck, J. Nagl, C. Callegari and W.E. Ernst, *Phys. Rev. Lett.* **101** (3), 035301–1–4 (2008).
 59 [29] J. Nagl, G. Auböck, A.W. Hauser et al., *Phys. Rev. Lett.* **100** (6), 063001–1–4 (2008).
 60 [30] M. Koch, G. Auböck, C. Callegari and W.E. Ernst, *Phys. Rev. Lett.* **103** (3), 035302–1–4 (2009).
 [31] M. Koch, J. Lanzersdorfer, C. Callegari et al., *J. Phys. Chem. A* **in press** (2009).
 <<http://dx.doi.org/10.1021/jp9041827>>.
 [32] Y. Takahashi, K. Fukuda, T. Kinoshita and T. Yabuzaki, *Z. Phys. B* **98** (3), 391–393 (1995).
 [33] T. Eichler, R. Müller-Siebert, D. Nettels et al., *Phys. Rev. Lett.* **88** (12), 123002–1–4 (2002).
 [34] T. Furukawa, Y. Matsuo, A. Hatakeyama et al., *Phys. Rev. Lett.* **96** (9), 095301–1–4 (2006).
 [35] P. Kusch, S. Millman and I.I. Rabi, *Phys. Rev.* **57** (9), 765–780 (1940).
 [36] E. Arimondo, M. Inguscio and P. Violino, *Rev. Mod. Phys.* **49** (1), 31–75 (1977).

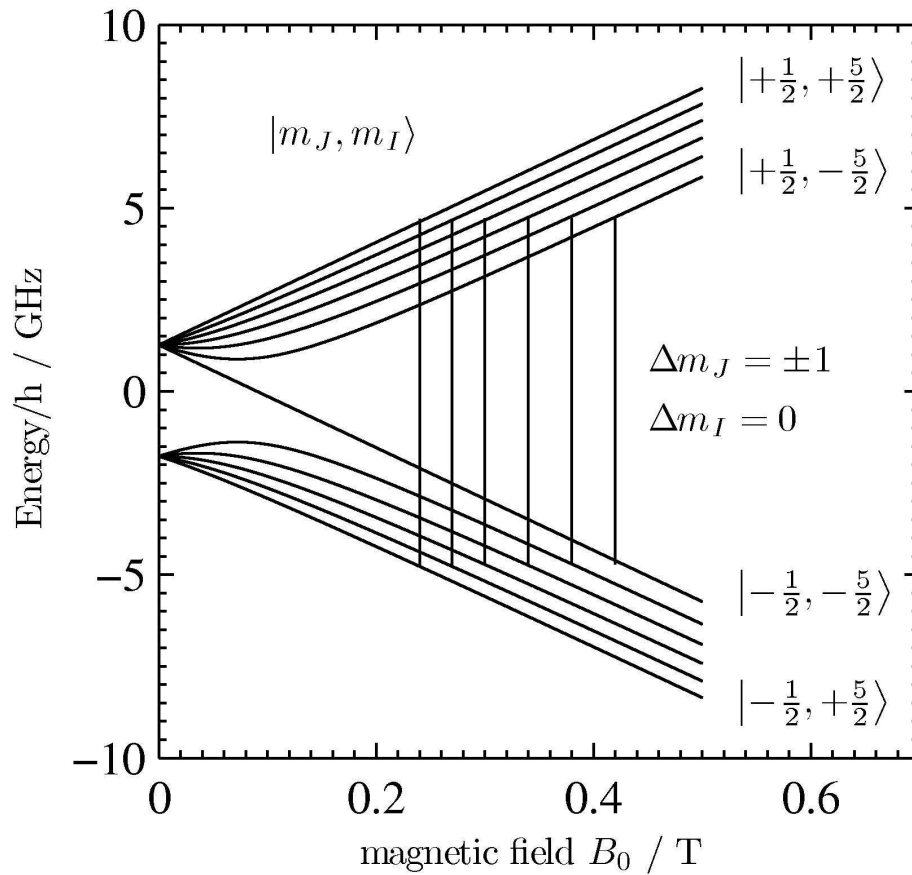
- 1 [37] W.E. Ernst and S. Kindt, *Appl. Phys. B* **31** (2), 79–83 (1983).
2 [38] F. Stienkemeier, J. Higgins, C. Callegari *et al.*, *Z. Phys. D* **38** (3), 253–263 (1996).
3 [39] F.R. Brühl, R.A. Trasca and W.E. Ernst, *J. Chem. Phys.* **115** (22), 10220–10224 (2001).
4 [40] Y. Ralchenko, A. Kramida, J. Reader and NIST ASD Team, NIST atomic spectra database, v. 3.1.5
5 online 2009. <<http://physics.nist.gov/asd3>>.
6 [41] J. Harms, J.P. Toennies and F. Dalfovo, *Phys. Rev. B* **58** (6), 3341–3350 (1998).
7 [42] C. Callegari and F. Ancilotto in preparation (2009).
8 [43] S.H. Patil, *J. Chem. Phys.* **94** (12), 8089–8095 (1991).
9 [44] F.J. Adrian, *J. Chem. Phys.* **32** (4), 972–981 (1960).
10 [45] N. Bloembergen, E.M. Purcell and R.V. Pound, *Phys. Rev.* **73** (7), 679–712 (1948).
11 [46] U. Kleinekathöfer, M. Lewerenz and M. Mladenović, *Phys. Rev. Lett.* **83** (23), 4717–4720 (1999).
12
13
14
15
16
17
18
19
20
21
22
23
24
25
26
27
28
29
30
31
32
33
34
35
36
37
38
39
40
41
42
43
44
45
46
47
48
49
50
51
52
53
54
55
56
57
58
59
60

For Peer Review Only



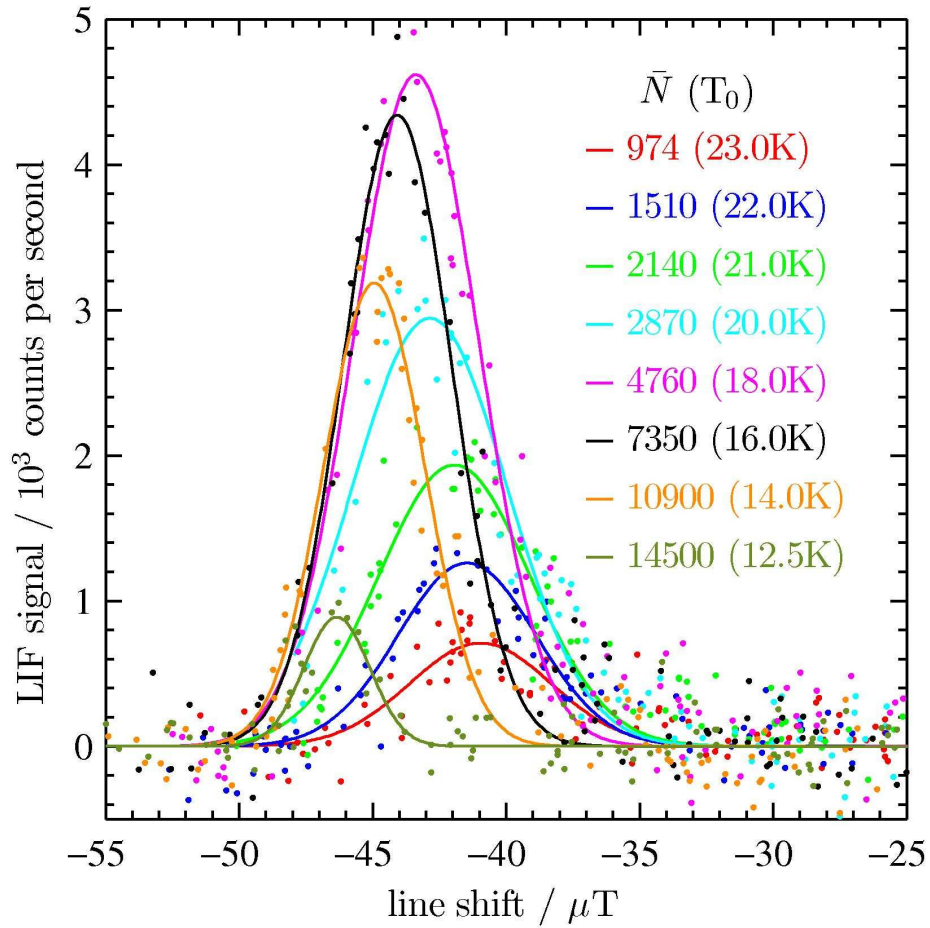
75x49mm (600 x 600 DPI)

Review Only



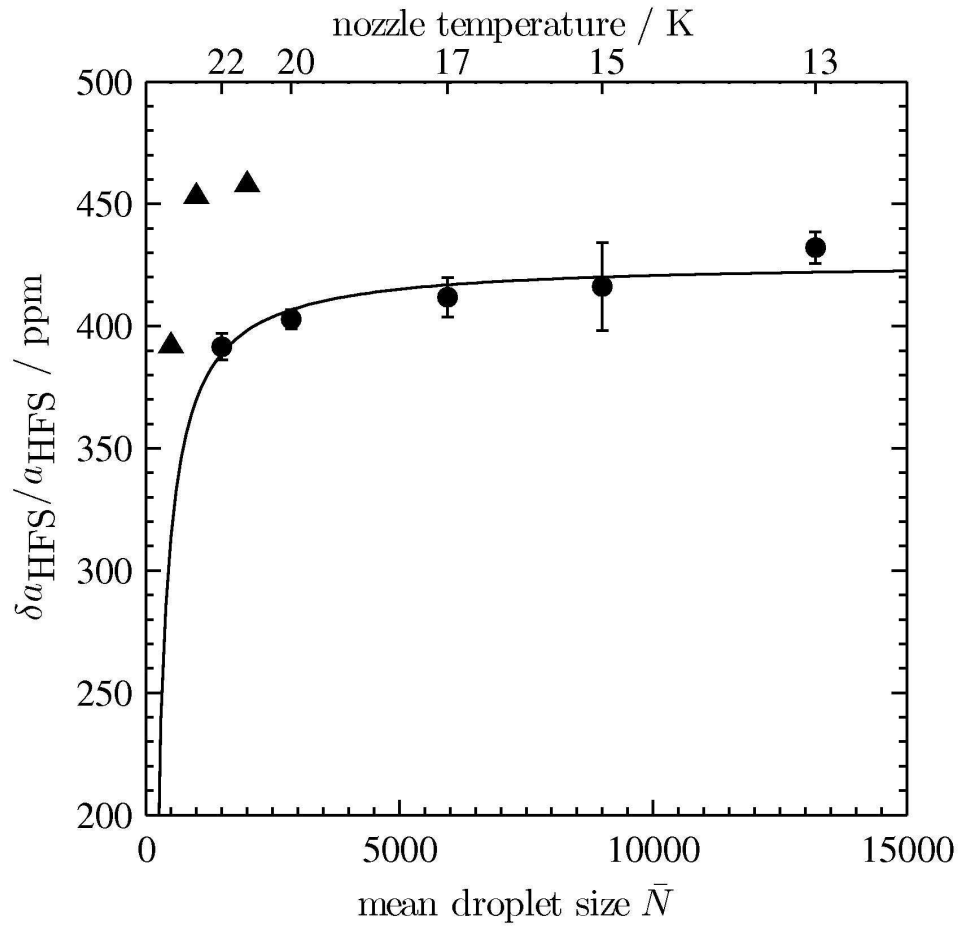
75x75mm (600 x 600 DPI)





75x75mm (600 x 600 DPI)





75x75mm (600 x 600 DPI)

